Chemical Process Design Vol.2 No.2 (2023) 22-36

University of Sistan and Baluchestan

Chemical Process Design

Available online at http://cpd.usb.ac.ir/



Electrochemical Determination of Drugs in Human Plasma Sample using a Modified Nanosensor

Ziaeddin Jafari[1], Abdolrasoul Pouranfard[1,*], Negin Rahimi[2]

[1] Department of Chemical Engineering, Yasouj University, Yasouj, Iran
[2] Tehran Uniersity of Medical Sciences, Tehran, Iran

ARTICLE INFO

Article history:
Received: 2023-07-02
Received in revised form: 2023-10-20
Accepted: 2023-12-20
Published online: 2023-12-20

Keywords:
TiO_2 nanosheet hierarchical spheres;
Electro catalytic properties;
Electrochemical impedance;
Spectroscopy;
Phenobarbital

DOI: *10.22111/CPD.2023.46054.1028*

ABSTRACT

An extremely sensitive and selective electrochemical sensor based on anatase TiO2 nanosheet hierarchical spheres (TiO_2NSHSs), Pt nanoparticles (PtNPs), carbon paste electrode (CPE) and 2,3-dihydro-2-(3,4-dihydroxyphenyl) quinazolin-4(1H)-one (DHP) for determination of isoprenaline (IP) in the presence of phenobarbital (PB) was developed. The excellent synergistic effect of TiO_2NSHSs, PtNPs and DHP showed significantly enhanced electro catalytic activity for IP and PB. In order to characterize the developed nanosensor, the scanning electron microscope (SEM), electrochemical impedance spectroscopy (EIS) and voltammetry were used. Electrochemical behavior of the DHP/PtNPs/TiO_2NSHSs/CPE sensor studied using differential pulse voltammetry (DPV), cyclic voltammetry (CV) and EIS. Several effective parameters were investigated and optimized on the nanosensor response. The proposed sensor, under the optimized conditions, showed two linear dynamic ranges from 0.05- 20.0 µM and 20.0-900.0 µM with a low detection limit of 7.0 nmol.L −1 for IP determination. Finally, the modified sensor was employed to determine the analytes in human blood plasma with ±0.3% error. Validation of the proposed method was performed using high-performance liquid chromatography (HPLC).

1. Introduction

Phenobarbital (PB) is known as a long-acting barbiturate and the most extensively used as the oldest demulcent [1]. Also, it was applied in the therapy of all types of seizures except absence type. PB was used for alcohol and benzodiazepine detoxification for its anodyne and anticonvulsant properties [2]. The long-time use of PB lead to the various adverse effects [3]. Sedation and hypnosis are the main side effects of PB [4]. The feature of PB toxicity leads to a “slowing” of bodily functions, such as bradycardia, hypothermia, decreased consciousness (even coma), bradypnea, and hypotension (in massive overdoses) [5].

Corresponding author. Tel.: +0098-074-31005068.
E-mail address: r.pouranfard@yu.ac.ir (A. Pouranfard)

Overdose may also cause to pulmonary edema and critical renal failure because of shock and might even lead to death [6]. Therefore, simple, rapid and cheap assays to aid clinical diagnostics is necessary. For quantitative PB determination, various techniques including: high-performance liquid chromatography (HPLC) [7], potentiometric method [8] and capillary electrophoresis [9] have been used. All of these techniques need costly equipment, trained person to operate and sample preparation in the most of them is time-consuming. Contrary to the techniques mentioned, the electrochemical methods are simple, rapid, high sensitive and low cost for the analysis of biological compounds and xenobiotics such as drugs [10–14]. Recently, the electrochemical biosensors have been so developed that are considered as the matter of basic as well as applied researches for nearly fifty years. Today, with the development of nanotechnology, nanomaterials, especially metal nanoparticles (MNPs), play an unavoidable role to improve the performance of the sensors [15–19].

Studies demonstrated that the electrochemical biosensors, which are modified with nanomaterials, can improve electrical signal for detection of biological compounds and xenobiotics with high over potential and low intensity [20,21]. In comparison with the bulk material; nanoparticles may have modified physical properties due to their size [22,23]. For this reason, nanostructured devices displayed some improved properties, such as enhanced catalytic activity or sensitivity. During these years, titanium and its composites have been extensively used in biosensors, batteries, solar cells, additives in toothpaste, white paint and others [24]. TiO_2NSHSs have been used due to the particular structure and distinctive properties, such as excellent electrical conductivity, extremely high mechanical strength and chemical stability. These unique characteristics make TiO_2NSHSs appropriate candidate for the modification of electrodes [25–27].

Electroanalytical chemists are very interested in using the platinum nanoparticles (PtNPs) as a matrix of sensors because of their excellent conducting capability, high surface-to-volume ratio, good biological compatibility and unique structural and catalytic properties. PtNPs are more stable than the commonly used Au nanoparticles, and they can be stored more efficiently and longer [28]. Recently, many research studies have been conducted on Pt NPs for various electrochemical applications, such as biosensors, bioassays, chemical sensors, and electrocatalysis [29–33]. The electrocatalytic activity of TiO_2 nanoparticles depends not only on the properties of the TiO_2 nanomaterial, but also depends on the material that is to be modified. It has been reported, for example, the combination of TiO_2 NSHSs with Pt NPs, which combines the advantages of these nanoparticles, can improve the electrocatalytic effect of these nanomaterials [34,35]. The combination of different nanostructures of TiO_2 NSHSs with Pt NPs can lead to novel composite materials and devices with appropriate properties for a wide spectrum of functional and biomedical applications [35].

In this study, as a novel work, the carbon paste electrode (CPE) was modified with TiO_2 NSHSs, noble metal Pt nanoparticles and DHP. Pt NPs on the surface of TiO_2 NSHSs significantly enhance the electrocatalytic activity of the semiconductor nanoparticles. This process has the best efficacy resulting charge separation between the electrons which accumulate on the metal and holes remaining on the electrocatalyst surface [36]. In addition, the modified electrodes were characterized by scanning electron microscopy (SEM) and electrochemical techniques. Also, the simultaneous IP and PB in the water and human blood serum samples were determined using the developed method. The lower limit of detection and short time of the procedure are great features of the DHP/PtNPs/TiO_2NSHSs/CPE electrode for determination of IP and PB.

2. Experimental

2.1. Materials and methods

In this work, all solutions were freshly prepared with double distilled water. Isoprenaline (IP) and phenobarbital (PB) obtained from Fluka. Hexachloroplatinic acid ($H_2PtCl_6.6H_2O$, Sigma-Aldrich), $NaBH_4$ (Merck), diethylenetriamine (DETA; 99%, Sigma-Aldrich), ethanol (EtOH, Merck, 99.8%), titanium isopropoxide ($Ti(OCH(CH_3)_2)_4$), 98%, Aldrich) and other reagents were prepared with analytical grade. Phosphate buffered solutions (PBS) 0.1 M in the pH range of 2.0–11.0 were prepared by mixing stock solutions of H_3PO_4–NaH_2PO_4 and NaH_2PO_4- Na_3PO_4. Graphite powder (provided by Merck company) and high viscosity paraffin oil (Merck, density = 0.88 g cm^{-3}) were used as binding agents for graphite pastes.

The morphological characterization has been carried out using a transmission electron microscope (TEM, Zeiss-EM10C at 80 KV) and scanning electron microscope (SEM, VEGA 3 SEM). XRD patterns were recorded on a Bruker D8 ADVANCE X-ray diffractometer using nickel-filtered Cu Kα radiation (λ= 1.5406 Å). The electrochemical measurements were performed with a potentiostat/galvanostat Ivium stat. A Metrohm 691 pH/ion meter was used to read the pH of the buffered solutions. A three-electrode cell was used at 25±1º C. Carbon paste electrode (CPE), TiO_2 nanosheet hierarchical spheres carbon paste electrode (TiO_2NSHSs/CPE), PtNPs/TiO_2NSHSs/CPE and DHP/PtNPs/TiO_2NSHSs/CPE were used as working electrodes. An Ag/AgCl (KCl, sat.) electrode and a platinum wire were used as a reference and auxiliary respectively.

2.2. Pt-nanoparticles preparation

In the experiments, the hexacholoroplatinate was reduced to metallic Pt with sodium borohydride in an aqueous solution and the PtNPs were obtained. The details of the procedure have been reported in literatures [37,38]. Briefly, 50 mL of doubly distilled water was used to dissolve H_2PtCl_6 (final concentration of H_2PtCl_6 was 3.4 mM) and 20.0 mM $NaBH_4$ was added to the prepared H_2PtCl_6 solution under vigorous stirring. After two hours, the Pt NPs were separated from the reaction mixture and washed three times with double distilled water. Finally, the purified PtNPs were dried under vacuum. The resulting PtNPs were ground and kept at 4 °C before using in the modification of electrode surface.

2.3. Synthesis of TiO_2 NSHSs

The hydrothermal method was used for the synthesis of TiO_2 NSHSs using titanium isopropoxide and diethylenetriamine (DETA) as starting materials [39]. Briefly, the titanium isopropoxide/diethylenetriamine precursor solution was prepared by adding 0.03 mL of DETA in 42 mL of isopropyl alcohol (IPA) using vigorous magnetic stirrer for a few minutes. Then 1.5 mL of titanium isopropoxide was added, and the solution was gently stirred at room temperature. The precursor solution was then immediately transferred into a teflon-lined stainless-steel autoclave with a volume of 150 mL for the hydrothermal reaction. The autoclave was placed at 200 °C for a 24 h in an electric oven and left to cool naturally to room temperature. The resulting white precipitate was gained via centrifugation, washed with deionized water and ethanol several times to eliminate the organic residues. The powder was then dried at 60 °C overnight and finally calcined at 400 °C with a heating rate of 1 °C min^{-1} for 2 h to achieve a highly crystalline anatase phase.

2.4. Electrode preparation

To achieve the best conditions in the preparation of DHP/PtNPs/TiO_2NSHSs/CPE, the ratio of DHP, TiO_2 NSHSs, and Pt NPs optimized. The findings of our research showed the maximum peak in current intensity for IP and PB. The DHP/PtNPs/TiO_2NSHSs/CPE were prepared by dissolving 0.02 g DHP in 1 mL chloromethane and then added in 0.9 g graphite powder, 0.040 g TiO_2 NSHSs and 0.040 g Pt NPs with a mortar and pestle. Then, to obtain a uniformly wetted paste, 0.6 mL of paraffin oil were added to the above mixture and mixed for 20 min. After blending, the paste was packed into the end of a glass tube. A copper wire was inserted through the opposite end to establish an electrical contact. Before the experiment, the surface of the prepared electrode was polished with fine paper. For comparison, other electrodes were prepared in the same way, such as DHP modified CPE electrode (DHP/CPE) without TiO_2 NSHSs and Pt NPs, TiO_2 NSHSs carbon paste electrode (TiO_2NSHSs/CPE) without DHP and Pt NPs, PtNPs/TiO_2NSHSs/CPE without DHP and unmodified CPE in the absence of DHP, TiO_2 NSHSs, and Pt NPs.

3. Results and discussion

3.1. Pt NPs characterization

The formation of Pt NPs has been confirmed via TEM measurements and absorption spectra. The aqueous solution of $PtCl_6^{2-}$ and aqueous suspension of Pt nanoparticles have been shown in Fig. 1. As seen in Fig. 1, a broad UV-vis absorption spectrum with a shoulder at 250 nm was observed for $PtCl_6^{2-}$ [40]. However, this peak was disappeared after formation of PtNPs. Inset of Fig. 1 displays a representative TEM image of the PtNPs obtained in aqueous solution. The presence of Pt quasi-spherical with a particle size of about 20 nm is confirmed.

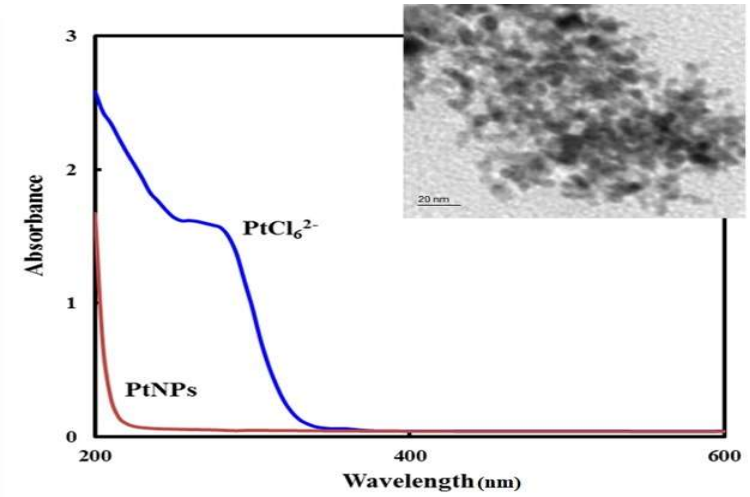


Fig. 1. Absorption spectrum of H2PtCl6 and PtNPs. Inset shows TEM image of the particles at a magnification of 100 nm

3.2. Description of Anatase TiO_2 NSHSs

The formation of TiO_2NSHSs that was evaluated by scanning electron microscope (SEM) and powder X-ray diffraction (XRD, PANanalytical Xpert Pro), have been shown in Fig. 2A,B. Anatase TiO_2 NSHSs were obtained by calcining the synthesized amine-stabilized TiO_2 NSHSs solvothermally, in a stagnant air with 400 °C. According to the Fig. 2A, it can be observed that TiO_2 NSHSs consists of micro-sized particles with a spherical morphology. The TiO_2 particles are connected to each other in the film. It is instantly apparent that the spheres are completely uniform,

with an average size of ~500nm. The surface of the sphere is very rough and appears fluffy. The XRD pattern of the material (Fig. 2B) shows that the as-prepared TiO_2 powder is anatase with a tetragonal structure. The XRD results are in parallel with the results reported in other literature [27,39].

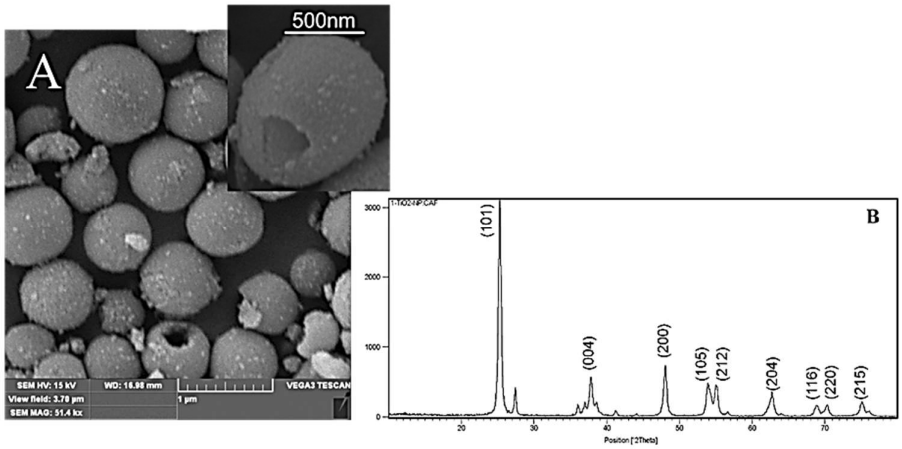


Fig. 2. SEM image of the synthesized TiO_2NSHSs (A), XRD patterns of the TiO_2NSHSs (B)

3.3. Characterization of surface morphology

The selective and sensitive detection of the target analyte by an electrode is significantly affected by its surface morphology. The changes in the surface morphology of electrodes after surface modification were examined by scanning electron microscopic (SEM) technique, and the results have been shown in Fig. 3A-C. The results indicated that at the surface of the unmodified CPE (Fig. 3A), the irregularly shaped flakes of graphite powders, that have been isolated from each other and some holes or cavities on the electrode surface has been presented because carbon paste is a porous material.

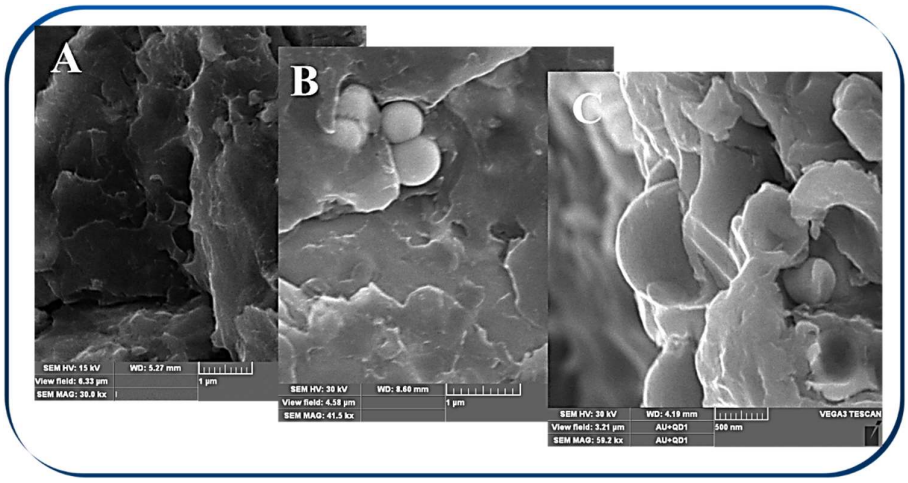


Fig. 3. SEM images of the CPE (A), TiO_2NSHSs/CPE (B) and PtNPs-TiO_2NSHSs/CPE (C)

These phenomena lead to the decrease of active surface area. After addition of PtNPs and TiO_2 NSHSs to carbon paste, these nanomaterials successfully were distributed on the electrode surface with three-dimensional spatial structures (Fig. 3B and Fig. 3C). Fig. 3C indicated that the CPE was successfully modified by the suggested nanomaterials. Also, Fig. 3C confirmed that the nanomaterial modifier was distributed nearly uniform at the carbon

surface which leads to filling the holes between the graphite layers and a larger surface area compared to unmodified CPE. Significant improvement in the surface structure of PtNPs/TiO_2NSHSs/CPE was observed.

3.4. Characterization by electrochemical impedance spectroscopy (EIS)

Data on the charge-transport and charge-transfer process in sensors can be measured by EIS. In a typical impedance spectrum, a semicircle part at higher frequencies correspond to the electron transfer-limit process, and a straight line at the lower frequencies correlated with the diffusion-limit process. The semicircle diameter of the impedance spectra at high frequency gave the charge transfer resistance (R_{CT}) [41]. To investigate the conducting nature of CPE, TiO_2NSHSs/CPE, and PtNPs/TiO_2NSHSs/CPE electrodes, electrochemical impedance spectroscopy (EIS) was used. Fig. 4 presented the Nyquist plots obtained for these electrodes in PBS (100 mM, pH 7.0, 0.9% NaCl) solution containing 5.0 mM $[Fe(CN)_6]^{3-/4-}$. It could be seen that on the CPE the value of RCT was obtained at 2170.0 Ω (curve a), which was due to the presence of non-conductive liquid paraffin in the carbon paste. Afterward, TiO_2 NSHSs had been added into the carbon paste to get a TiO_2NSHSs/CPE, the value of RCT was decreased to 970.0 Ω (curve b).

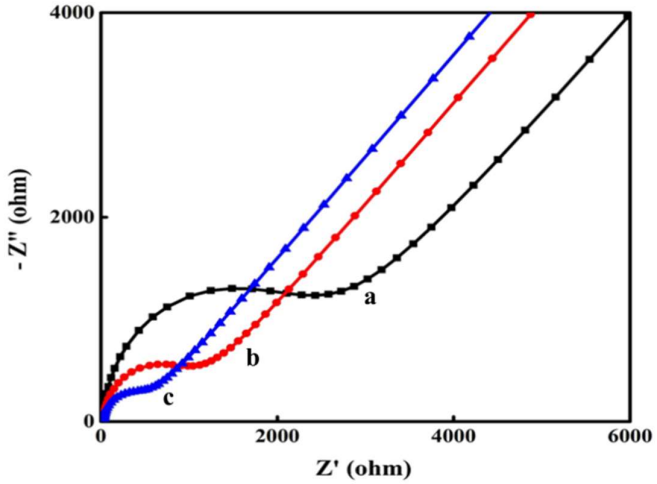


Fig. 4. Nyquist plots for (a) Bare CPE, (b) TiO_2NSHSs/CPE and (c) PtNPs-TiO_2NSHSs/CPE electrodes in PBS (100 mM, pH=7.0, 0.9% NaCl) solution containing 5.0 mM [Fe (CN)6]3−/4− at scanning frequencies from 0.01 to 100000 Hz

These results suggest that the lower RCT of the TiO_2NSHSs/CPE is due to the availability of more TiO_2 NSHSs in the film, which leads to enhanced electrical conductivity. Also, the large surface area of the TiO_2 NSHSs implies that the nanosheets are probably not rigid packed such that a greater surface area is exposed. This phenomenon leads to the facile electron transfer reaction and accordingly accelerates the diffusion of ferricyanide towards the TiO_2NSHSs/CPE surface. After modification of TiO_2NSHSs/CPE with PtNPs the electron transfer resistance value is dramatically decreased compared to TiO_2NSHSs/CPE (curve c 425.0 Ω), which indicates that TiO_2NSHSs/CPE is effectively modified with Pt NPs and thus increases the rate of electron transfer between an electrode surface and $[Fe(CN)_6]^{3-/4-}$. Because of the high surface area of the Pt NPs on the electrode surface (PtNPs/TiO_2NSHSs/CPE), an enhancement in the sensitivity of the electrode was observed.

3.5. Electrochemical properties of modified DHP/PtNPs/TiO$_2$NSHSs/CPE

To the best of our knowledge, the electrochemical properties and, especially, the electrocatalytic activity of DHP in aqueous solution were not reported up to now. Therefore, in this work, the modified electrodes based on DHP-PtNPs-TiO$_2$NSHSs/CPE were prepared, and their electrochemical properties in a buffer aqueous solution (pH = 7.0) using cyclic voltammetry have been studied. It should be noted that the DHP as an electrode modifier, in aqueous media is insoluble and this is a great advantage. The cyclic voltammetric (CV) studies done at various potential scan rates (υ, 10 to 800 mV/s in 0.1 M PBS (pH = 7.0)) to investigate the interfacial kinetics on the DHP/PtNPs/TiO2NSHSs/CPE surface (Fig. 5). By increasing in the scan rate, the anodic and cathodic peaks of electrodes shift in opposite directions, suggesting the redox process to be quasi-reversible. The peak potential as a logarithmic function of potential scan rate varied linearly in the range of 10 to 800 mV/s, and has been represented in Fig. 5 (inset A). From Laviron's equations, the value of transfer coefficient (α), for n number of electrons, can obtain from the slope of two straight lines with cathodic and anodic slopes of −2.303RT/αnF and 2.303RT/(1−α)nF, respectively. The average transfer coefficient (α) is calculated as 0.49. The charge transfer rate constant (ks= 2.7 s^{-1}) is calculated using Eq. **Error! Reference source not found.** [42].

$$logks = \alpha log(1-\alpha) + (1-\alpha) log\alpha - log(RT/n\alpha Fv) - \alpha(1-\alpha) n\alpha F\Delta Ep/2.3RT \quad (1)$$

An approximate estimate of the surface coverage of the electrode, the surface concentration of electroactive species can be estimated using Eq. **Error! Reference source not found.** [42].

$$Ip = n^2F^2A\Gamma v/4RT \quad (2)$$

where n is the number of electrons involved in the reaction, A is the surface area (0.0962 cm^2) of the electrode, Γ (mol cm^{-2}) is the surface coverage, and the other symbols have their usual meanings. From the slope of the anodic peak currents versus the scan rate (Fig. 5, inset B), the calculated surface concentration is = 1.11 × 10^{-7} mol cm^{-2} for n = 2.

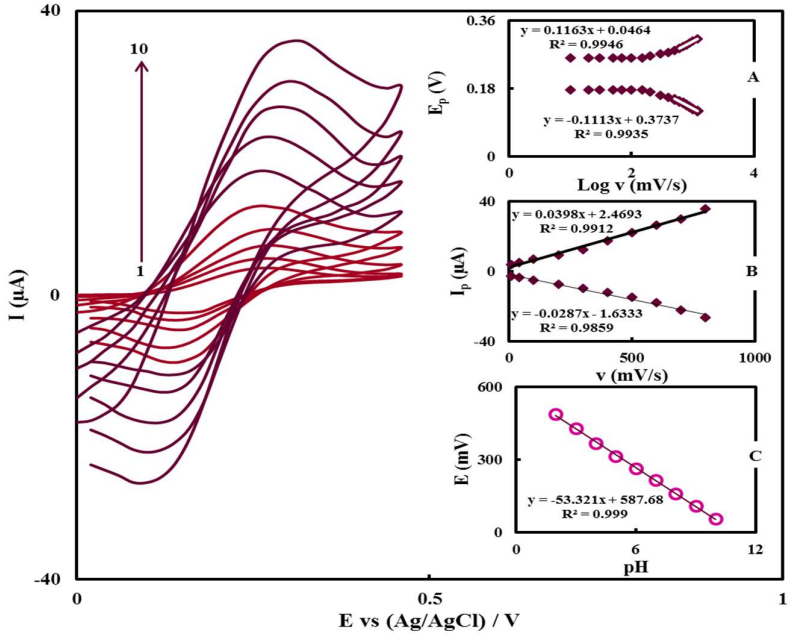


Fig. 5. Cyclic voltammograms of DHP-PtNPs-TiO$_2$NSHSs/CPE in buffer solution (pH=7.0) for different scan rates; the letters 1–10 correspond to: 10, 40,100, 200, 300, 400, 500, 600, 700 and 800 mVs-1. Insets (A): Plot of peak potentials versus the logarithm of the potential scan rate in the range of 10 - 800 mVs-1, (B) Ip vs. scan rate and (C) Epa, Epc, E1/2 vs. pH

The electrochemical behavior of DHP/PtNPs/TiO_2NSHSs/CPE was studied at different pHs using CV. The results indicated that by increasing pH, the anodic and cathodic peak potentials of DHP at PtNPs-TiO_2NSHSs/CPE shifted to negative values. By plotting the anodic, cathodic and half-wave potential values as the function of pH, the potential-pH diagrams have been shown in Fig. 5(C). The average of the anodic and cathodic peak potentials of the cyclic voltammograms [(Epa+Epc)/2] were calculated as the half-wave potentials ($E_{1/2}$) [43]. The three plots were straight lines with slopes near 53.3 mV/pH, and this indicated that the system obeyed the Nernst equation for a two-electron and proton transfer reaction [44].

The electroactive surface area (A_e) for the modified electrodes can be calculated by the linear slope of the anodic peak currents versus the square root of potential sweep rates. For CPE, TiO_2NSHSs/CPE and PtNPs-TiO_2NSHSs/CPE electrodes, Ae was obtained by using the calculated diffusion coefficient and a distinct concentration of $[Fe(CN)_6]^{3-/4-}$ via the Randles−Sevick equation as follows [44]

$$Ip = \left(2.69\times10^5\right)\alpha^{1/2}n^{3/2}F^2ACD^{1/2}/\nu^{1/2} \quad (1)$$

where C is the molar concentration of $[Fe(CN)_6]^{3-/4-}$, and A is the electrode surface area, n is the electron transfer number, D is the diffusion coefficient and ν is the scan rate. For the mentioned electrodes, using 5.0 mM solution of $[Fe(CN)_6]^{3-/4-}$ in PBS (100.0 m M, pH=7.0, 0.9% NaCl) and the slope obtained from the linear regression of Ip versus $\nu^{1/2}$, the Ae was calculated. The value of A_e for CPE, TiO_2NSHSs/CPE and PtNPs-TiO_2NSHSs/CPE were obtained 0.093 cm^2, 0.325 cm^2 and 1.028 cm^2, respectively. The results indicated that the presence of TiO_2 NSHSs and Pt NPs together increased the active surface of electrodes.

3.6. Electrochemical behaviors of IP and PB on proposed electrodes

To investigate the roles of TiO_2 NSHSs, Pt NPs and DHP in CPE for the electrochemical oxidation of IP and PB, the electrochemical behaviors of the target analytes at different electrodes have been investigated, and results using cyclic voltammetry method have been displayed in Fig. 6A-D.

The comparison of electrocatalytic oxidation toward IP and PB at the surface of different working electrodes has been shown in **Error! Reference source not found.** The TiO_2 NSHSs/CPE exhibited a well-defined irreversible oxidation peak at 365 mV, and 650 mV for oxidation of IP and PB, respectively (Fig. 6B), whereas the CPE electrode provided a weak irreversible oxidation peak (Fig. 6A). The peak potential due to the oxidation of IP at the surface of PtNPs/TiO_2NSHSs/CPE occurs at 340 mV, which was about 65 mV and 25 mV more negative than CPE and TiO_2NSHSs/CPE, respectively. Also, the peak potential due to the oxidation of PB occurs at 615 mV, which was about 104 mV and 29 mV more negative than CPE and TiO_2NSHSs/CPE, respectively (Fig. 6C). The higher enhanced peak current indicated an enhanced electron transfer rate for IP and PB at PtNPs/TiO_2NSHSs/CPE. The presence of TiO_2NSHSs and PtNPs had a great improvement on the electrochemical response, which was partly due to excellent characteristics of TiO_2NSHSs and PtNPs such as high surface area, relatively good conductivity, and high chemical stability. TiO_2NSHSs as an electrocatalyst and PtNPs as a good electrical conductor, thereby making the oxidation IP and PB more facile at the electrode surface. No cathodic peak was seen on the reverse scan of potential within the investigated potential range because IP and PB oxidation are an electrochemically irreversible process at the surface of these electrodes.

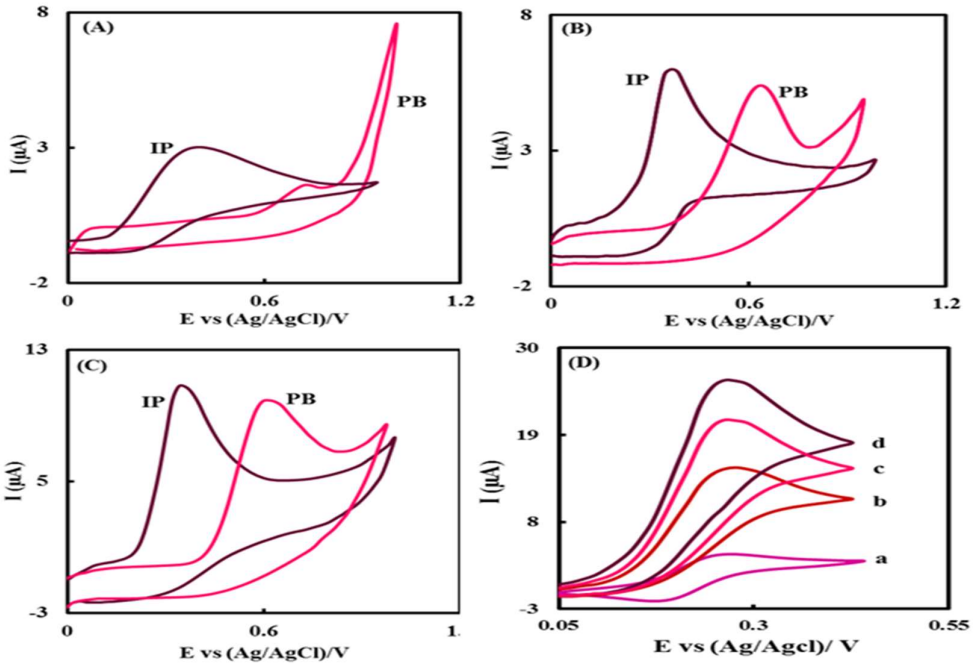


Fig. 6. Cyclic voltammograms of IP (40.0 µM) and PB (50.0 µM) at (A) bare CPE, (B) TiO_2NSHSs/CPE and (C) PtNPs-TiO_2NSHSs/CPE. (D) CVs obtained for the oxidation of 80.0 µM of IP at (b) DHP/CPE, (c) DHP-TiO_2NSHSs/CPE, (d) DHP-PtNPs-TiO_2NSHSs/CPE and curve (a) show the CV of blank solution at the DHP-PtNPs-TiO_2NSHSs/CPE. In the all cases: Electrolyte: 0.1 M PB solution (pH=7.0), scan rate: 30 mVs^{-1}

Table 1. Values of cyclic voltammetric parameters at the surface of different modified electrodes for IP and PB

Parameter	CPE		TiO_2NSHSs/CPE		nPt/TiO_2NSHSs/CPE		DHP/nPt/TiO_2NSHSs/CPE
	IP	PB	IP	PB	IP	PB	IP
E_{pa}(mV)	405	725	365	650	340	615	261
I_{pa}(µA)	3.01	1.80	5.82	5.39	10.77	9.85	14.22

The anodic peak potential for IP oxidation at the surface of DHP/PtNPs/TiO_2NSHSs/CPE electrode with enhanced oxidation current was 261 mV (Fig. 6D). Also, the results showed (Fig. 6D) that the peak potential of IP oxidation at the DHP/PtNPs/TiO_2NSHSs/CPE electrode was shifted by 79, 104 and 144 mV towards negative values compared with the PtNPs/TiO_2NSHSs/CPE, TiO_2NSHSs/CPE and the unmodified CPE, respectively. Comparison of the curves (a) and (d) of Fig. 6D, presented that the anodic peak current at the surface of DHP/PtNPs/TiO_2NSHSs/CPE was considerably enhanced by the addition of IP to the solution and the cathodic peak current completely disappeared. DHP acted as a mediator in carbon paste matrix for voltammetric determination of IP and PB. These results suggested that an electrocatalytic behavior for IP oxidation at the surface of DHP/PtNPs/TiO_2NSHSs/CPE via an EC catalytic mechanism. Fig. 7 illustrated the schematic representation of the possible reaction pathways for electrooxidation of IP and PB on PtNPs/TiO_2NSHSs/CPE in 0.1 M phosphate buffer solution (pH = 7.0).

3.7. Differential pulse voltammetry measurements

Differential pulse voltammetry (DPV) has better characteristics and higher sensitivity for analytical applications. Therefore, in this study, DPV was used to investigate the electrochemical response of the fabricated DHP/PtNPs/TiO_2NSHSs/CPE electrode in phosphate buffer solution containing various concentrations of IP and PB. The linear range and detection limit of IP in the absence and presence of PB were calculated.

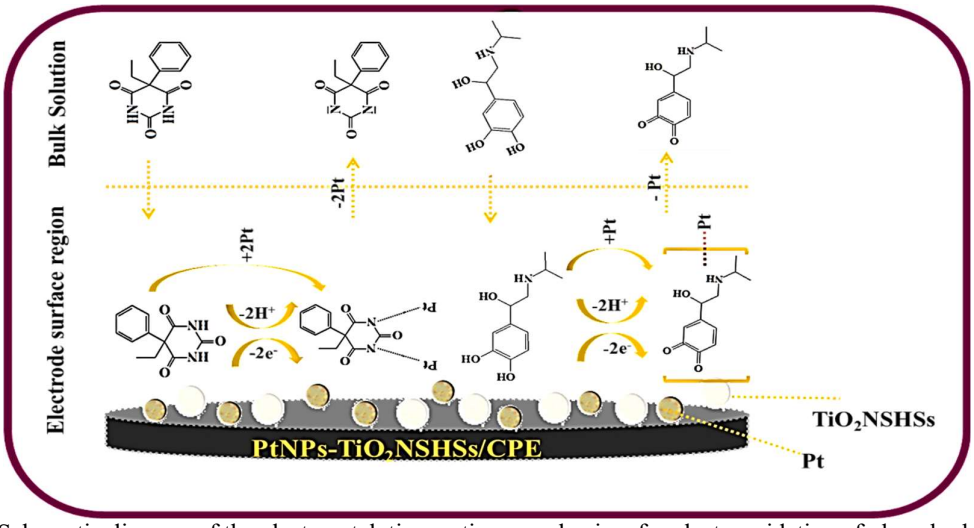


Fig. 7. Schematic diagram of the electrocatalytic reactions mechanism for electrooxidation of phenobarbital and isoprenaline at the surface of PtNPs-TiO_2NSHSs/CPE

The plot of peak versus IP concentration yielded two calibration plots corresponding to two concentration ranges of 0.05- 20.0 µM and 20.0-900.0 µM with slopes of 0.678 and 0.051 µA μM^{-1}, respectively (Fig. 8). The detection limit was obtained as 7.0 nM using the calibration equation of first linear segment.

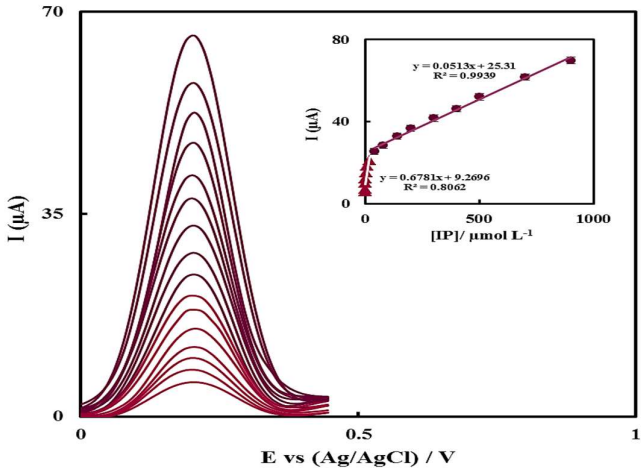


Fig. 8. DPVs of DHP-PtNPs-TiO_2NSHSs/CPE in 0.1 M PBS (pH=7.0) containing different concentrations of IP. The numbers of 1–16 correspond to: 0.05, 0.1, 0.5, 1.0, 5.0, 10.0, 20.0, 40.0, 80.0, 140.0, 200.0, 300.0, 400, 500.0, 600, 700.0, 800 and 900.0 µM of IP. Insets show the plot of the electrocatalytic peak current as a function of IP concentration in the ranges of 0.05 to 20.0 µM and 20.0 to 900.0 µM

Furthermore, DPV was employed for the simultaneous determination of IP and PB at DHP/PtNPs/TiO_2NSHSs/CPE. Well-defined oxidation peaks were observed for IP and PB at 0.18, 0.60 and vs. Ag/AgCl, respectively (Fig. ***9***). The results indicated that the DHP/PtNPs/TiO_2NSHSs/CPE was highly appropriate for the simultaneous determination of the IP and PB in a mixture. When the concentrations of IP and PB increased, the peak currents of the respective analytes enhanced, linearly. Fig. 9 shows the corresponding peak current vs. analyte concentration (calibration plots) for IP and PB. The obtained sensitivity of the modified electrode towards the oxidation of IP in the presence of PB (0.5505 and 0.0635 µA μM^{-1}) was very close to the value observed in the absence of PB (0.678 and 0.051 µA μM^{-}

[1]). Therefore, the oxidation processes of IP and PB at DHP/PtNPs/TiO_2NSHSs/CPE were independent, and the simultaneous determination of the two analytes was possible without any interference.

The detection limit and linear range were achieved as 2.0 µM and 5.0–300.0 µM for IP and 2.6 µM and 8.0–350.0 µM for PB. The improved characteristics have been obtained for the fabricated electrode can be attributed to the presence of TiO_2 NSHSs and Pt nanoparticles that promoted electron transfer from the electrode surface to analytes. Due to providing a high surface to volume ratio, these results are expected from TiO_2 NSHSs and Pt nanoparticles. Finally, enhancement of the effective surface area available for signal transduction led to the improved detection limit. To assess the repeatability of DHP/PtNPs/TiO_2NSHSs/CPE, the oxidation of 30.0 µM IP was recorded using DPV for 10 measurements at physiological pH solution.

The relative standard deviation of 10 successive scans was reported as 1.6% that confirmed appropriate reproducibility of the modified electrode. For evaluation of the reproducibility of the results, five different DHP/PtNPs/TiO_2NSHSs/CPE electrodes were fabricated under similar conditions. Their current response and peak potential toward the oxidation of IP and PB were the same at all five electrodes. The calculated RSD for DPV peak current was about 2.4 % for IP. This occurrence indicated that the reproducibility of electrode preparation was acceptable. Furthermore, after being stored for 2 weeks, the response to 30.0 µM IP decreased by only 6%, indicated the suitable stability of DHP/PtNPs/TiO_2NSHSs/CPE.

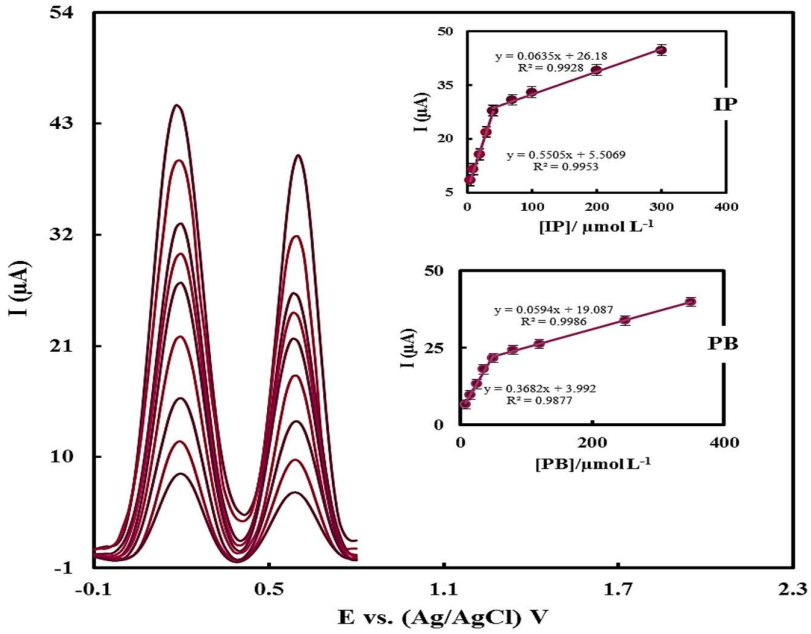


Fig. 9. DPVs of DHP-PtNPs-TiO_2NSHSs/CPE in phosphate buffer (pH=7.0) containing different concentrations of IP and PB: from inner to outer corresponds to mixed solutions of 5.0 +8.0, 10.0+15.0, 20.0+25.0, 30.0+35.0, 40.0+50.0, 70.0+80.0, 100.0+120.0, 200.0+250.0 and 300.0+350.0 µM where the first value is the concentration of IP and the second value is the concentration of PB. Insets: (A) and (B) are calibration plots of IP and PB respectively; scan rate: 20 mVs^{-1}, pulse amplitude: 0.05 V and pulse width: 0.05 s.

3.8. Interference studies

Under the optimal conditions for determination of IP and PB, interferences of some substances that exist in biological liquids were investigated. The allowable limit was taken as the maximum concentration of the foreign substances, which caused an approximately ±5% relative error. The interference tests were carried out by the DPV technique in

the presence of 20 µM IP and 20 µM PB. The tolerated concentration of foreign substances was 1.0×10^{-1} M for Na^{+}, K^{+}, Ca^{2+}, $SO4^{2-}$, NO^{3-}, Cl^{-}, Br^{-}, S^{2-}, CO^{3-}, CH_3COO^{-}. The experimental results for other interfering agents within the same concentration level of IP and PB have been given in Table 2. Results showed that there was little change response in the IP and PB signals when these substances were added to the electrolyte solution. It could be seen that the presence of this species at a given concentration did not interfere with determination of IP and PB. It was confirmed that the DHP/PtNPs/TiO_2NSHSs/CPE could be considered as a suitable electrochemical sensor for recognition of IP and PB.

Table 2. Effect of different interferences on the voltammetric signal of IP and PB at DHP/nPt/TiO_2NSHSs/CPE

Interfering agent	Concentration (µM)	Signal average for 20 µM IP	Signal average for 20 µM PB	Signal Change (%)	
				IP	PB
Absence of interferences	20 µM IP +20 µM PB	15.65 µA	11.400 µA	-	-
Alanine	20.0	15.70 µA	11.41 µA	+0.3	+0.05
Arginine	30.0	15.85 µA	11.401 µA	+1.3	0.01
Aspartic acid	60.0	15.68 µA	11. 400 µA	+0.2	~0.0
Citric acid	40.0	15.82 µA	11. 400 µA	+1.1	~0.0
Folic acid	100.0	16.00 µA	11.45 µA	+2.3	+0.4
Uric acid	100.0	15.88 µA	11.43 µA	+1.5	+0.3
L-asparagine	40.0	15.96 µA	11.41 µA	+2.0	0.05
L-lysine	50.0	15.74 µA	11.401 µA	+0.6	0.01
Glutamic acid	70.0	15.68 µA	11.400 µA	+0.2	~0.0
Serine	70.0	15.73 µA	11.402 µA	+0.5	~0.02
Threonine	70.0	15.79 µA	11.400 µA	+0.9	~0.0
Valine	70.0	15.82 µA	11.400 µA	+1.1	~0.0
Leucine	50.0	16.02 µA	11.403 µA	+2.4	0.03
Glycine	50.0	15.93 µA	11.401 µA	+1.8	0.01
L-tryptophan	50.0	15.76 µA	11.53 µA	+0.7	+1.1
L-tyrosine	50.0	15.66 µA	11.400 µA	+0.1	~0.0

3.9. Use of DHP/PtNPs/TiO_2NSHSs/CPE for recovery and determination of IP and PB in real samples

Because of evaluation of the utilization of suggested sensor in clinical investigations, DHP/PtNPs/TiO_2NSHSs/CPE was used for determination of IP and PB in diluted blood serum samples and synthetic solutions using standard addition method. Different amounts of IP and PB spiked to three diluted serum samples (diluted with phosphate buffer solution pH = 7.0). The prepared samples were analyzed by the DHP/PtNPs/TiO_2NSHSs/CPE five times. Results of determined IP and PB in synthetic solutions and serum samples have been given in Table 3, which showed satisfactory recovery percent.

The concentrations of IP and PB in serum samples were analyzed using the HPLC technique [45–47], and the results agreed with the values measured using HP/PtNPs/TiO_2NSHSs/CPE electrode. Results indicated that determination of IP and PB in blood serum samples could be successfully performed by the proposed novel method. Also, five synthetic mixture solutions containing different concentrations of IP and PB were prepared by phosphate buffer solution (pH 7.0). Each of the samples was analyzed by DPV five times, and average recovery percent was obtained.

Table 3. Simultaneous determination of the IP and PB in synthetic solutions and diluted blood serum samples and the amounts of IP and PB in blood serum samples determined by HPLC technique

Sample		Spiked (µM)		Proposed Method, Recovery% (±SD for n=5)		HPLC Method, Recovery% (±SD for n=3)	
		IP	PB	IP	PB	IP	PB
Serum Blood Samples	1	5.0	25.0	98.0 ±0.6	103.6 ± 0.5	101.5± 0.7	103.3± 0.2
	2	10.0	35.0	99.3 ±0.1	101.5 ± 0.6	97.7± 0.5	104.0± 0.5

	3	15.0	50.0	103.2±0.5	97.3 ± 0.4	103.5± 0.2	101.2± 0.6
	4	20.0	80.0	102.8±0.4	98.4 ± 0.2	98.5± 0.3	98.5± 0.4
	5	25.0	120.0	97.9 ±0.3	101.6 ± 0.5	97.6± 0.6	96.4± 0.5
Synthetic Solutions	1	5.0	8.0	101.0 ±0.5	102.2 ± 0.5		
	2	10.0	15.0	103.3 ±0.6	98.6 ± 0.7		
	3	20.0	25.0	97.5 ±0.4	103.4 ± 0.8		
	4	30.0	35.0	104.1 ±0.3	97.1± 0.4		
	5	40.0	50.0	101.7 ± 0.4	103.5 ± 0.3		

4. Conclusion

This work demonstrated a simple, facile, and reproducible method for the construction of a DHP/PtNPs/TiO_2NSHSs/CPE electrode and its application for the simultaneous determination of IP and PB for the first time. The combination of TiO_2 NSHSs and Pt nanoparticles can increase electrode surface and enhance electronic and catalytic properties. According to the experimental data, DHP/PtNPs/TiO_2NSHSs/CPE had a high efficiency and indicated two well-defined redox peaks for oxidation of IP and PB, which were large enough to determine IP and PB individually and in the presence of each other. The oxidation peak currents obtained using DPV were linearly dependent on IP and PB concentrations and the detection limits for IP and PB were 0.33 and 0.57 μM, respectively. The application of DHP/PtNPs/TiO_2NSHSs/CPE electrode in the analysis of real samples for simultaneous determination of IP and PB was evaluated with high sensitivity and excellent performance. Moreover, the electrochemical response of present modified electrode had not a significant change, so that this procedure could be used for the fabrication of stable sensors for the selective determination of electroactive analytes.

References

[1] Hosgood, J.R., Kimbrel, J.M., Protus, B.M.C., Grauer, P.A., 2016, Evaluation of Subcutaneous Phenobarbital Administration in Hospice Patients, American Journal of Hospice and Palliative Medicine, 33(3), 209–213. https://doi.org/10.1177/1049909114555157

[2] Bialer, M., Chemical properties of antiepileptic drugs (AEDs), Advanced drug delivery reviews, 64(10), 887–895. https://doi.org/10.1016/j.addr.2011.11.006

[3] Perucca, P., Gilliam, F.G., 2012, Adverse effects of antiepileptic drugs, The Lancet Neurology, 11(9), 792–802. https://doi.org/10.1016/S1474-4422(12)70153-9

[4] Yasiry, Z., Shorvon, S.D., 2012, How phenobarbital revolutionized epilepsy therapy: The story of phenobarbital therapy in epilepsy in the last 100 years, Epilepsia, 53(s8), 26–39. https://doi.org/10.1111/epi.12026

[5] Koufaris, C., Wright, J., Osborne, M., Currie, R.A., Gooderham, N.J., 2013, Time and dose-dependent effects of phenobarbital on the rat liver miRNAome, Toxicology, 314(2-3), 247–253. https://doi.org/10.1016/j.tox.2013.10.004

[6] Brodie, M.J., Kwan, P., 2012, Current position of phenobarbital in epilepsy and its future, Epilepsia, 53(s8), 40–46. https://doi.org/10.1111/epi.12027

[7] Asadi, M., Dadfarnia, S., Shabani, A.M.H., Abbasi, B., 2015, Simultaneous extraction and quantification of lamotrigine, phenobarbital, and phenytoin in human plasma and urine samples using solidified floating organic drop microextraction and high-performance liquid chromatography, Journal of Separation Science, 38(14), 2510–2516. https://doi.org/10.1002/jssc.201500237

[8] Lima, J.L.F.C., Montenegro, M.C.B.S.M., Da Silva, A.M.R., 1990, A phenobarbital ion-selective electrode without an inner reference solution, and its application to pharmaceutical analysis, Journal of Pharmaceutical and Biomedical Analysis, 8(8-12), 701–704. https://doi.org/10.1016/0731-7085(90)80106-Y

[9] Haque, A., Xu, X., Stewart, J.T., 1999, Determination of ephedrine, theophylline and phenobarbital in a tablet dosage form by capillary electrophoresis, Journal of Pharmaceutical and Biomedical Analysis, 21(5), 1063–1067. https://doi.org/10.1016/S0731-7085(99)00226-5

[10] Hasanzadeh, M., Pournaghi-Azar, M.H., Shadjou, N., Jouyban, A., 2014, Determination of diltiazem in the presence of timolol in human serum samples using a nanoFe_3O_4@GO modified glassy carbon electrode, RSC Advances, 4(93), 51734–51744. https://doi.org/10.1039/C4RA05989A

[11] Unal, D.N., Eksin, E., Erdem, A., 2018, Electrochemical determination of 6-thioguanine and its interaction with DNA oligonucleotides using disposable graphite pencil electrodes, Analytical Letters, 51(1-2), 265–278. https://doi.org/10.1080/00032719.2017.1338714

[12] Norouzi, P., Haji-Hashemi, H., Larijani, B., Aghazadeh, M., Pourbasheer, E., Ganjali, M.R., 2017, Application of new advanced electrochemical methods combine with nano-based materials sensor in drugs analysis, Current Analytical Chemistry, 13(1), 70-80. https://doi.org/10.2174/1573411012666160601150841

[13] Thapliyal, N., Chiwunze, T.E., Karpoormath, R., Goyal, R.N., Patel, H., Cherukupalli, S., 2016, Research progress in electroanalytical techniques for determination of antimalarial drugs in pharmaceutical and biological samples, RSC advances, 6(62), 57580–57602. https://doi.org/10.1039/C6RA05025E
[14] Mahmoudi, E., Hajian, A., Rezaei, M., Afkhami, A., Amine, A., Bagheri, H., 2019, A novel platform based on graphene nanoribbons/protein capped Au-Cu bimetallic nanoclusters: Application to the sensitive electrochemical determination of bisphenol A, Microchemical Journal, 145, 242-251. https://doi.org/10.1016/j.microc.2018.10.044
[15] Zhao, H., Liu, F., Wu, S., Yang, L., Zhang, Y.P., Li, C.P., 2017, Ultrasensitive electrochemical detection of Dicer1 3′UTR for the fast analysis of alternative cleavage and polyadenylation, Nanoscale, 9(12), 4272–4282. https://doi.org/10.1039/C6NR09300K
[16] Wang, Z., Dai, Z., 2015, Carbon nanomaterial-based electrochemical biosensors: An overview, Nanoscale, 7(15), 6420–6431. https://doi.org/10.1039/C5NR00585J
[17] Liu, S., Zhang, J., Tu, W., Bao, J., Dai, Z., 2014, Using ruthenium polypyridyl functionalized ZnO mesocrystals and gold nanoparticle dotted graphene composite for biological recognition and electrochemiluminescence biosensing, Nanoscale, 6(4), 2419–2425. https://doi.org/10.1039/C3NR05944H
[18] Yadav, M., Ganesan, V., Gupta, R., Yadav, D.K., Sonkar, P.K., 2019, Cobalt oxide nanocrystals anchored on graphene sheets for electrochemical determination of chloramphenicol, Microchemical Journal, 146, 881-887. https://doi.org/10.1016/j.microc.2019.02.025
[19] Yue, H.Y., Wu, P.F., Huang, S., Gao, X., Song, S.S., Wang, W.Q., Guo, X.R., 2019, Simultaneous electrochemical determination of levodopa and uric acid based on ZnS nanoparticles/3D graphene foam electrode, Microchemical Journal, 149, 103977. https://doi.org/10.1016/j.microc.2019.103977
[20] Veseli, A., Mullallari, F., Balidemaj, F., Berisha, L., Švorc, L., Arbneshi, T., 2019, Electrochemical determination of erythromycin in drinking water resources by surface modified screen-printed carbon electrodes, Microchemical Journal, 148, 412-418. https://doi.org/10.1016/j.microc.2019.04.086
[21] Ateş, A.K., Er, E., Çelikkan, H., Erk, N., 2019, The fabrication of a highly sensitive electrochemical sensor based on AuNPs@graphene nanocomposite: Application to the determination of antidepressant vortioxetine, Microchemical Journal, 148, 306-312. https://doi.org/10.1016/j.microc.2019.04.082
[22] Lin, C.A.J., Liedl, T., Sperling, R.A., Fernández-Argüelles, M.T., Costa-Fernández, J.M., Pereiro, R., Sanz-Medel, A., Chang, W.H., Parak, W.J., 2007, Bioanalytics and biolabeling with semiconductor nanoparticles (quantum dots), Journal of Materials Chemistry, 17, 1343–1346. https://doi.org/10.1039/B618902D
[23] Gill, R., Zayats, M., Willner, I., 2008, Semiconductor quantum dots for bioanalysis, Angewandte Chemie International Edition, 47, 7602–7625. https://doi.org/10.1002/anie.200800169
[24] Dumitriu, C., Popescu, M., Ungureanu, C., Pirvu, C., 2015, Antibacterial efficiencies of TiO_2 nanostructured layers prepared in organic viscous electrolytes, Applied Surface Science, 341, 157–165. https://doi.org/10.1016/j.apsusc.2015.02.183
[25] Rahman, M.M., Alfonso, V.G., Fabregat-Santiago, F., Bisquert, J., Asiri, A.M., Alshehri, A.A., Albar, H.A., 2017, Hydrazine sensors development based on a glassy carbon electrode modified with a nanostructured TiO_2 films by electrochemical approach, Microchimica Acta, 184, 2123–2129. https://doi.org/10.1007/s00604-017-2228-x
[26] Sun, W., Zhai, Z., Wang, D., Liu, S., Jiao, K., 2009, Electrochemistry of hemoglobin entrapped in a Nafion/nano-ZnO film on carbon ionic liquid electrode, Bioelectrochemistry, 74(2), 295–300. https://doi.org/10.1016/j.bioelechem.2008.11.001
[27] Wang, H., Liu, M., Yan, C., Bell, J., 2012, Reduced electron recombination of dye-sensitized solar cells based on TiO_2 spheres consisting of ultrathin nanosheets with [001] facet exposed, Beilstein journal of nanotechnology, 3, 378-387. https://doi.org/10.3762/bjnano.3.44
[28] Islam, A., Anwarul Kabir Bhuiya, M., Saidul Islam, M., 2014, A Review on Chemical Synthesis Process of Platinum Nanoparticles, Asia Pacific Journal of Energy and Environment, 1(2), 107-121. https://doi.org/10.18034/apjee.v1i2.215
[29] Govindhan, M., Liu, Z., Chen, A., 2016, Design and Electrochemical Study of Platinum-Based Nanomaterials for Sensitive Detection of Nitric Oxide in Biomedical Applications, Nanomaterials, 6(11), 211. https://doi.org/10.3390/nano6110211
[30] Borisova, B., Sánchez, A., Jiménez-Falcao, S., Martín, M., Salazar, P., Parrado, C., Pingarrón, J.M., Villalonga, R., 2016, Reduced graphene oxide-carboxymethylcellulose layered with platinum nanoparticles/PAMAM dendrimer/magnetic nanoparticles hybrids. Application to the preparation of enzyme electrochemical biosensors, Sensors and Actuators B: Chemical, 232, 84–90. https://doi.org/10.1016/j.snb.2016.02.106
[31] Willinger, E., Tarasov, A., Blume, R., Rinaldi, A., Timpe, O., Massué, C., Scherzer, M., Noack, J., Schlögl, R., Willinger, M.G., 2017, Characterization of the Platinum-Carbon Interface for Electrochemical Applications, ACS Catalysis, 7(7), 4395–4407. https://doi.org/10.1021/acscatal.7b00614
[32] Liu, X., Chen, N., Han, B., Xiao, X., Chen, G., Djerdj, I., Wang, Y., 2015, Nanoparticle cluster gas sensor: Pt activated SnO_2 nanoparticles for NH_3 detection with ultrahigh sensitivity, Nanoscale, 7, 14872–14880. https://doi.org/10.1039/C5NR03585F
[33] Gaikwad, N., Bhanoth, S., More, P.V., Jain, G.H., Khanna, P.K., 2014, Chemically designed Pt/PPy nano-composite for effective LPG gas sensor, Nanoscale, 6, 2746–2751. https://doi.org/10.1039/C3NR05375J
[34] Liu, L., Miao, P., Xu, Y., Tian, Z., Zou, Z., Li, G., 2010, Study of Pt/TiO_2 nanocomposite for cancer-cell treatment, Journal of Photochemistry and Photobiology B: Biology, 98(3), 207–210. https://doi.org/10.1016/j.jphotobiol.2010.01.005
[35] Ding, Y., Wang, Y., Zhang, L., Zhang, H., Li, C.M., Lei, Y., 2011, Preparation of TiO_2-Pt hybrid nanofibers and their application for sensitive hydrazine detection, Nanoscale, 3, 1149–1157. https://doi.org/10.1039/C0NR00773K
[36] Kasarevic-Popovic, Z., Behar, D., Rabani, J., 2004, Role of excess electrons in TiO_2 nanoparticles coated with Pt in reduction reactions studied in radiolysis of aqueous solutions, The Journal of Physical Chemistry B, 108(52), 20291–20295. https://doi.org/10.1021/jp045989g
[37] Choi, J.-H., Park, K.-W., Kwon, B.-K., Sung, Y.-E., 2003, Methanol Oxidation on Pt/Ru, Pt/Ni, and Pt/Ru/Ni Anode Electrocatalysts at Different Temperatures for DMFCs, Journal of The Electrochemical Society, 150(7), A973-A978.

https://doi.org/10.1149/1.1581011
[38] Chang, L.Y., Lee, C.P., Huang, K.C., Wang, Y.C., Yeh, M.H., Lin, J.J., Ho, K.C., 2012, Facile fabrication of PtNP/MWCNT nanohybrid films for flexible counter electrode in dye-sensitized solar cells, Journal of Materials Chemistry, 22, 3185–3191. https://doi.org/10.1039/C2JM15614H
[39] Chen, J.S., Zhu, T., Yang, X.H., Yang, H.G., Lou, X.W., 2010, Top-down fabrication of α-Fe_2O_3 single-crystal nanodiscs and microparticles with tunable porosity for largely improved lithium storage properties, Journal of the American Chemical Society, 132(38), 13162–13164. https://doi.org/10.1021/ja1060438
[40] Zheng, L., Xiong, L., Sun, J., Li, J., Yang, S., Xia, J., 2008, Capping agent free synthesis of PtSn bimetallic nanoparticles with enhanced electrocatalytic activity and lifetime over methanol oxidation, Catalysis Communications, 9(5), 624–629. https://doi.org/10.1016/j.catcom.2007.06.017
[41] Razmi, H., Mohammad-Rezaei, R., 2013, Graphene quantum dots as a new substrate for immobilization and direct electrochemistry of glucose oxidase: Application to sensitive glucose determination, Biosensors and Bioelectronics, 41, 498–504. https://doi.org/10.1016/j.bios.2012.09.009
[42] Laviron, E., 1979, General expression of the linear potential sweep voltammogram in the case of diffusionless electrochemical systems, Journal of Electroanalytical Chemistry and Interfacial Electrochemistry, 101(1), 19–28. https://doi.org/10.1016/S0022-0728(79)80075-3
[43] Geno, P.W., Ravichandran, K., Baldwin, R.P., 1985, Chemically modified carbon paste electrodes. Part IV. Electrostatic binding and electrocatalysis at poly(4-vinylpyridine)-containing electrodes, Journal of Electroanalytical Chemistry and Interfacial Electrochemistry, 183(1-2), 155–166. https://doi.org/10.1016/0368-1874(85)85488-5
[44] Bard, A.J., Faulkner, L.R., 2001, Electrochemical Methods: Fundamentals and applications, 2nd Edition. John Wiley & Sons, Inc.,
[45] Hjemdahl, P., Martinsson, A., Larsson, K., 1986, Improvement of the isoprenaline infusion test by plasma concentration measurements, Life sciences, 39(7), 629–635. https://doi.org/10.1016/0024-3205(86)90044-5
[46] Kishore, P., Rajnarayana, K., Reddy, M.S., Sagar, J.V., Krishna, D.R., 2003, Validated high performance liquid chromatographic method for simultaneous determination of phenytoin, phenobarbital and carbamazepine in human serum, Arzneimittelforschung, 53(11), 763–768. https://doi.org/10.1055/s-0031-1299826
[47] Franeta, J.T., Agbaba, D., Eric, S., Pavkov, S., Aleksic, M., Vladimirov, S., 2002, HPLC assay of acetylsalicylic acid, paracetamol, caffeine and phenobarbital in tablets, Il Farmaco, 57(9), 709–713. https://doi.org/10.1016/S0014-827X(02)01265-X